Dynamics of Ultra-Relativistic Nuclear Collisions with Heavy Beams: An Experimental Overview

Peter Braun-Munzinger
Gesellschaft für Schwerionenforschung
64220 Darmstadt, Germany
and
Johanna Stachel
Physikalisches Institut
Universität Heidelberg
69120 Heidelberg, Germany

We review, from an experimental point of view, the current status of ultra-relativistic nuclear collisions with heavy beams.

1. Introduction

Reactions between heavy nuclei at ultra-relativistic energies have now been studied for a number of years at the BNL AGS (11.4 GeV/nucleon) and at the CERN SPS (158 GeV/nucleon). Progress has been rapid but it is only in the last year that sufficiently complete and comprehensive data sets have become available that a "picture" is beginning to emerge. In the following we will briefly review the experimental highlights since the last Quark Matter conference at Heidelberg. Particular emphasis will be placed on the identification of possible collective behavior and hydrodynamic flow as well as on the question whether or not there is local equilibrium at freeze-out. As most progress since QM'96 in the leptonic sector will only be reported at this conference we will only touch upon recent experimental developments in the study of the low-mass dilepton continuum and very briefly summarize the status of anomalous charmonium suppression.

2. Global Variables

2.1. E_T and $dE_T/d\eta$ Distributions

Measurements of the transverse energy production and its spatial distribution in central Au+Au collisions at the AGS [1] and Pb+Pb collisions at the SPS [2] have yielded maximum pseudorapidity densities of $dE_T/d\eta$ = 200 and 450 GeV, respectively. Using a simple Bjorken-type estimate these values imply energy densities in the fireball formed in the collision of about 1.3 and 3 GeV/fm^3. Recent results from solutions of QCD on the lattice [3] imply critical temperatures (for systems including dynamical quarks) well below 200 MeV. The corresponding critical energy density is then of the order of 1-1.5 GeV/fm^3. The fireball's parameters discussed above are obviously in an interesting region.

2.2. N_c and $\mathrm{dN}_c/\mathrm{d}\eta$ Distributions

Pseudo-rapidity distributions of charged particles have been measured in Au+Au [4] and Pb+Pb [5] collisions over nearly the full solid angle. The total charged particle multiplicity in central collisions increases from about 450 at AGS energy to about 1500 at SPS energy. At AGS energy there are about equal numbers of pions and nucleons, while the pion to nucleon ratio is about 6 to 1 at SPS energy. This implies (within a thermal model, see below) a significant increase of the entropy per baryon in the fireball from about 15 to 38.

3. Spectral Distributions

Spectral distributions of high quality for protons and produced particles now exist [5–10] for heavy colliding systems both at AGS and SPS energy. In the following we will concentrate on the information on can glean from such spectra concerning stopping and, in particluar, the presence or absence of collective features such as hydrodynamic flow.

3.1. Rapidity Distributions and Baryon Stopping

The rapidity distribution of identified baryons has been measured over the full solid angle at AGS energy [6,7]. The distribution is approximately Gaussian in shape with a peak at central rapidity and a width significantly narrower than that observed for the system Si+Al, implying strong baryon stopping. A similar difference is observed for the net proton rapidity distributions in Pb+Pb and S+S collisions at SPS energy [5]. To get a complete picture here one has to await measurements of the Λ and $\bar{\Lambda}$ rapidity distributions. Current results from Na49 [11] are still somewhat controversial, with the Λ distribution nearly as narrow in rapidity as the $\bar{\Lambda}$ distribution. In any case, there is significantly increased stopping also at SPS energies, which is, of course, reflected in the increased entropy per baryon (see above).

3.2. Transverse Momentum Distributions

A general feature which has emerged from many measurements of transverse momentum distributions is that, especially for central collisions of heavy nuclei, the invariant distributions $d^2N/m_t dm_t dy$ which are approximately exponential in shape, i.e. $d^2N/m_t dm_t dy \propto \exp(-m_t/T)$, have inverse slope constants T increasing linearly with the mass of the particle under consideration. Since the transverse momentum $p_t = m\gamma_t\beta_t$ this fact has been widely interpreted as evidence for collective transverse flow: if there is a common flow velocity (or velocity profile) β_t superimposed on the random (thermal) motion of particles, the slope constant T, which is proportional to $\langle p_t \rangle$ increases linearly with m. One can, however, also reproduce many features of the measured spectra by assuming that the incoming nucleons undergo initial state scattering [12]. Since the amount of initial state scattering only depends on the number of nucleon-nucleon collisions each nucleon undergoes during the collision, hence is geometrical in nature, one does not need to invoke any collective expansion to explain the data in this approach. To resolve this issue, we discuss in some detail the two models and their implications.

3.2.1. Random Walk

The aim of the random walk model [12] is to provide a description of minimum bias data on transverse momentum distributions in proton-nucleus collisions by a superposition of the "kicks" the projectile nucleon undergoes in each nucleon-nucleon collision in the target nucleus. Since the extrapolation to AA collisions is then entirely geometric, one can test the predictions of this model directly by comparison to measured transverse momentum distributions. For pA collisions the approach is as follows. Each projectile nucleon undergoes N_A nucleon-nucleon collisions in the target. Since, averaged over impact parameter b, the nuclear thickness of the target is $4/3R_A$, where $R_A = 1.12A^{1/3}$fm is the radius of the target,

$$N_A = 4/3 R_A \sigma_{NN} n_0. \tag{1}$$

Here $n_0 = 0.17/\mathrm{fm}^3$ is the nuclear density and the total nucleon-nucleon cross section σ_{NN} is about 40 mb. One further assumes that each NN collision produces a fireball and that all final particles are emitted from the sequence of fireballs so created. Each fireball moves at a certain rapidity y and transverse momentum p_t, determined by a boost invariant longitudinal expansion scenario (for y) and by the history of NN "kicks" for p_t. To obtain the observed scaling with mass of the inverse slope constants the random walk proponents assume that the "kick" happens in transverse rapidity $\rho_t = 0.5\ln((m_t + p_t)/(m_t - p_t))$ rather than in p_t. Although this physically seems not obvious, it clearly introduces a "transverse velocity" distribution and, consequently, a mass dependent slope parameter. Since the sequence of kicks is stochastic, the distribution of the fireballs in transverse rapidity is assumed to be

$$f_{pA}(\rho_t) \propto \exp(-\rho_t^2/\delta_{pA}^2), \tag{2}$$

with

$$\delta_{pA}^2 = (N_A - 1)\delta_0^2. \tag{3}$$

Here, δ_0 is the only free parameter, apart from the fireball temperature (see below). It is determined by a fit to pA data and then kept constant for AB collisions.

Generalizing the above expressions to nucleus-nucleus collisions we replace δ_{pA} by

$$\delta_{AB}^2(b) = (N_c(b)/A + N_c(b)/B - 2)\delta_0^2 \tag{4}$$

with

$$N_c(b) = T_{AB}(b)\sigma_{NN}. \tag{5}$$

Here, the total number of collisions $N_c(b)$ for a given impact parameter b is evaluated with the help of the nuclear thickness function [13]. The purely geometrical nature of the problem becomes therefore transparent. Apart from a normalization factor which does not concern us here the expression for transverse mass spectra then reads:

$$\frac{dN^{AB}}{m_t dm_t} \propto \int d\rho \exp(-\rho^2/\delta_{AB}^2) g(m_t), \tag{6}$$

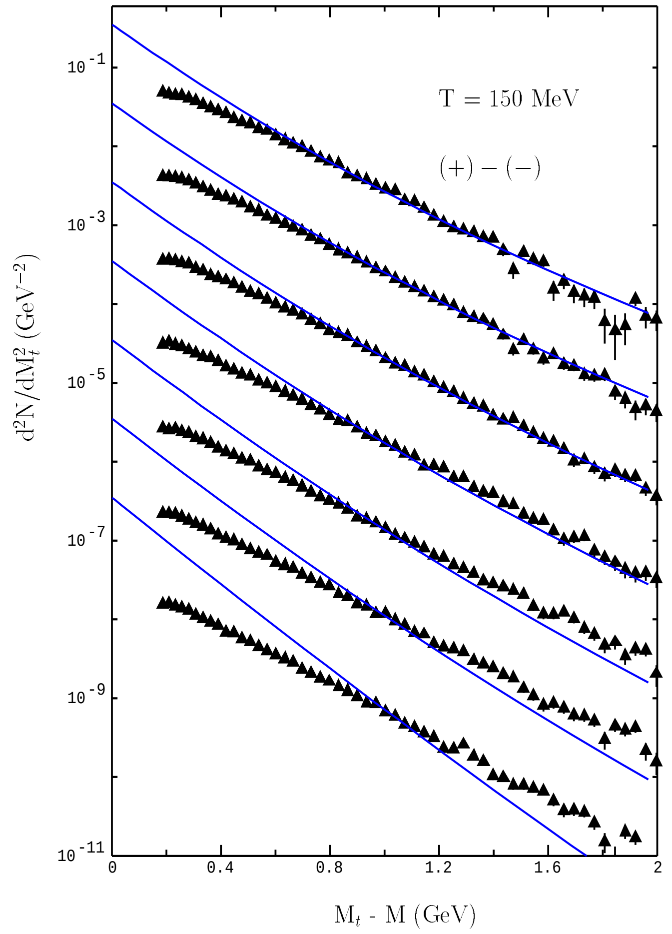

Figure 1.
Comparison of (+) - (-) spectra for Pb+Au collisions with predictions of the random walk model for different centralities (increasing centrality from bottom to top). The data are from the CERES collaboration [14].

where

$$g(m_t) = \int_{-y_L}^{y_L} dy m_t cosh(y - y_m) I_0(\frac{p_t sinh(\rho)}{T}) K_1(\frac{m_t cosh(y - y_m)}{T}). \tag{7}$$

Here, I_0 and K_1 are the modified Bessel functions and the particles are detected at rapidity y_m.

In the following, we will compare predictions according to Eq. (6) with recent data on "proton" transverse momentum distributions, *i.e.* the difference of the spectra distributions of positively and negatively charged particles, from the CERES collaboration [14]. These data for Pb+Au collisions were recorded with a multiplicity trigger corresponding to the upper 35 % of the geometrical cross section. This multiplicity range was subdivided into 7 exclusive intervals corresponding to (in a geometrical interpretation) mean impact parameters of 2, 2.5, 3.5, 4.3, 5.1, 6.0, and 7.4 fm, respectively. The data are shown in Fig. 1.Data in different multiplicity (or impact parameter) bins were multiplied by consecutive factors of 8. The lines in Fig. 1 correspond to predictions of the random walk model according to Eq. (6), with $\delta_0 = 0.146$. Since we are only interested in the shape of the distributions here, the normalization of the calculation relative to the data is arbitrary. Note that, for central collisions corresponding to mean impact parameters 3.5 fm and less, the calculated distributions reproduce the shape of the data very well in the range $0.7 < m_t - m < 2$ GeV. For more peripheral collisions, however, the predictions by the random walk model exhibit inverse slope constants which are considerably smaller than seen in the data. It is important to realize that there is no parameter to change here, as the centrality dependence is determined by the thickness of matter traversed. If one determines the inverse slope constants from a fit to both the data and the calculations in the range $0.6 < m_t - m < 2$ GeV one can make this comparison more quantitative, as shown in Fig. 2. Here, the discrepancy between data and calculations becomes very

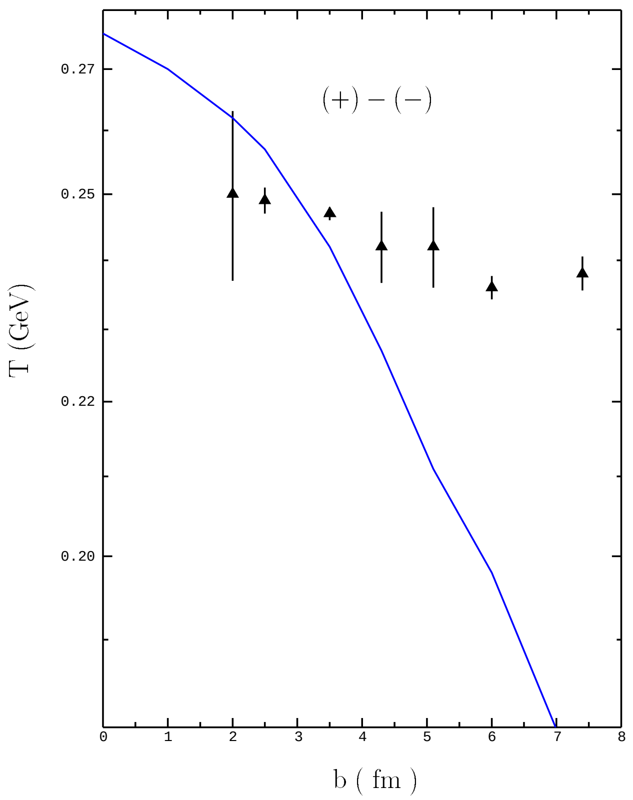

Figure 2.
Comparison of measured inverse slope constants and values calculated in the random walk model for different centralities. Data are from the CERES collaboration [14].

obvious: certainly in its present form the random walk prescription is not consistent with the observed very weak impact parameter dependence of inverse slope constants measured for protons in Pb+Au collisions at SPS energy. Taking into account further that the calculated spectra also deviate strongly from the data at lower $m_t - m$ values we conclude that the random walk model is not anymore a contender to describe the flow-like features observed in the transverse momentum spectra.

3.2.2. Transverse Flow

For central collisions, the transverse momentum spectra of all observed particles can be well described in a hydrodynamical approach. The basic equations for azimuthally symmetric flow, i.e. central collisions, are very similar to Eq. 6, except for the distributions in transverse rapidity. In a hydrodynamical approach, these distributions are obtained from the transverse flow velocity profile which, of course, depends on the initial conditions as well as on the underlying equation of state. We illustrate the success of this approach for data from the NA49 collaboration [11] in Figs. 3 and 4. The hydrodynamic calculations used the transverse velocity profile recently calculated by Alam et al. [15]. The initial conditions were chosen to reflect the measured charged particle multiplicities in central Pb+Pb collisions at SPS energy. For the equation of state it was assumed that a pure quark-gluon plasma undergoes a first order phase transition at $T_c = 160$ MeV to a hadronic resonance gas with freeze-out assumed to take place at constant temperature T_f. In Fig. 3 the data are compared to the calculations represented by the dashed lines for $T_f = 120$ MeV. Excellent agreement between the shape of the measured distributions and the calculations is obtained for all particle species ranging from pions to deuterons. We also show, in Fig. 3, the result of calculations with a linear profile $\tanh \rho_t = \beta_t = \beta_{max} \frac{r}{R_A}$. Again, good agreement between data and calculations is obtained for $T_f = 120$ MeV and $\beta_{max} = 0.6$. As is well known T_f cannot easily be determined from such fits, as higher T_f values can be traded off against lower β_t values. This is illustrated in Fig. 4 where the solid lines show the results of a calculation with $T_f = 140$ MeV and $\beta_t = 0.45$. We note, however, that the full hydrodynamic calculation does not exhibit this degeneracy: for $T_f = 140$ MeV, there is, with the present initial conditions and equation of state, no possibility to describe all measured distributions simultaneously. Under the assumptions discussed above, the data seem to clearly favor a relatively low freeze-out temperature near 120 MeV. The reason is that, to build up the flow in the hadronic phase, one needs the freeze-out to happen not too close to T_c. A similar conclusion was recently obtained by the NA49 collaboration from a simultaneous analysis of tranverse momentum spectra and two-pion interferometry data [16].

3.3. Azimuthal Anisotropy and Directed Flow

The study of collective flow effects via the experimental observation of anisotropies in azimuthal distributions for non-central collisions is motivated by theoretical predictions that a quark-gluon phase will lead to distinct differences in the flow patterns compared to what is expected for a hadron gas. Such phenomena were originally studied experimentally at Bevalac energies and below. With the advent of the heaviest beams at the AGS and SPS such effects were also established there [17,18], at first in distributions of global observables such at E_T and later also in distributions of identified particles. It is now customary to extract information on flow by determination of the Fourier coefficients v_i

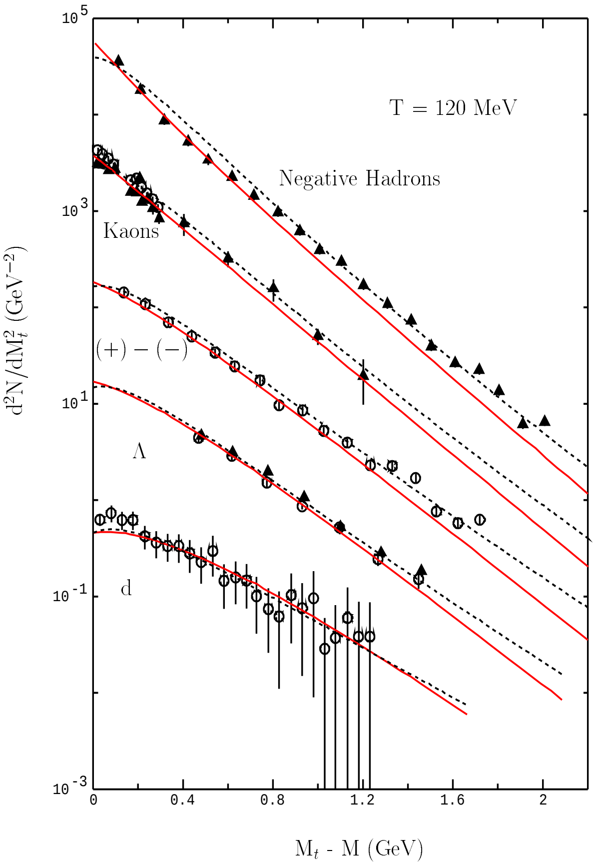

Figure 3.
Comparison of hydrodynamic calculations assuming a freeze-out temperature of 120 MeV with transverse momentum spectra for various particles. The data are from the NA49 collaboration [11] and are arbitrarily renormalized for clarity of presentation. The solid lines are calculations assuming a linear velocity profile. The dashed lines use the velocity profile determined by the initial conditions and the equation of state. For details see text.

of the azimuthal distributions $F(\phi)$ integrated over a certain rapidity interval

$$F(\phi) = F_0(1 + \sum_{i=1}^{n} 2v_i \cos(i\phi)). \tag{8}$$

The dipole coefficient v_1 is also denoted as 'directed flow' and is associated to the mean transverse momentum in the reaction plane $\langle p_x \rangle$ by

$$v_1 = \langle p_x \rangle / \langle p_t \rangle, \tag{9}$$

the quadrupole coefficient v_2 is also called 'elliptic flow'. The odd Fourier coefficients change sign at midrapidity, while the even coefficients are symmetric. A quantity that was used to characterize the directed flow is the change of $\langle p_x \rangle$ with rapidity in the vicinity

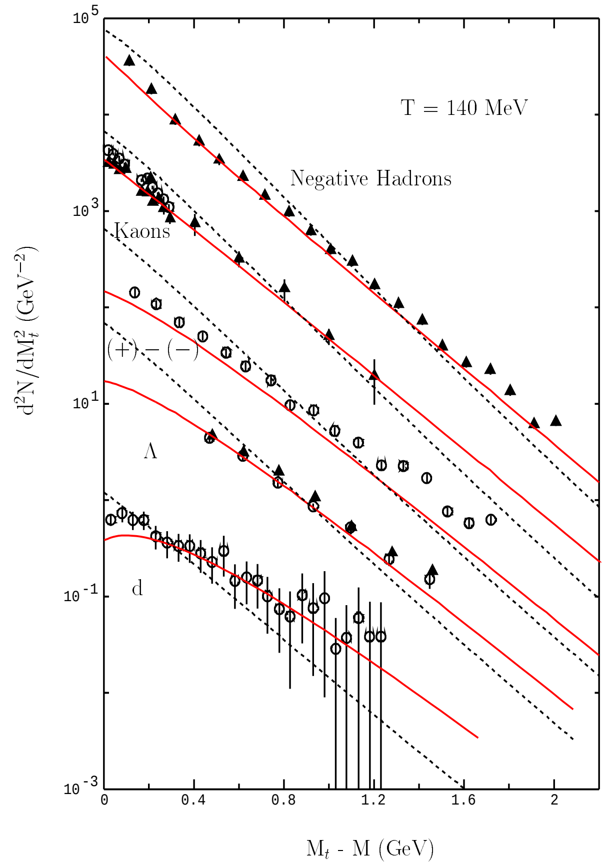

Figure 4.
Same as Figure 3 but for a freeze-out temperature of 140 MeV.

of mid-rapidity and indeed the quantity

$$F_y = d\langle p_x \rangle / dy \tag{10}$$

is scale invariant and should be independent of beam energy if there is no change in the physics. Fig. 5 displays the information on directed flow of protons in terms of this scale invariant variable as a function of the beam kinetic energy per nucleon. One can see a plateau in the beam energy range of a few hundred MeV to 1 GeV and a steep fall-off to much lower values at the AGS and again much lower values at the SPS. It should be noted that the baryon density reached in the collisions is maximal for the AGS regime while it is lower and of comparable magnitude for the high end of the Bevalac/SIS regime and the SPS. So, at a qualitative level, one can clearly state that there is a difference in the equation of state over the energy regime considered with an increasing softening at the higher energies.

It was shown at this conference [19] that the directed flow of light nuclei is larger than the proton flow and increases monotonically with particle mass. The pion and kaon flow on the other hand appear to be a complex superposition of Coulomb effects, strong

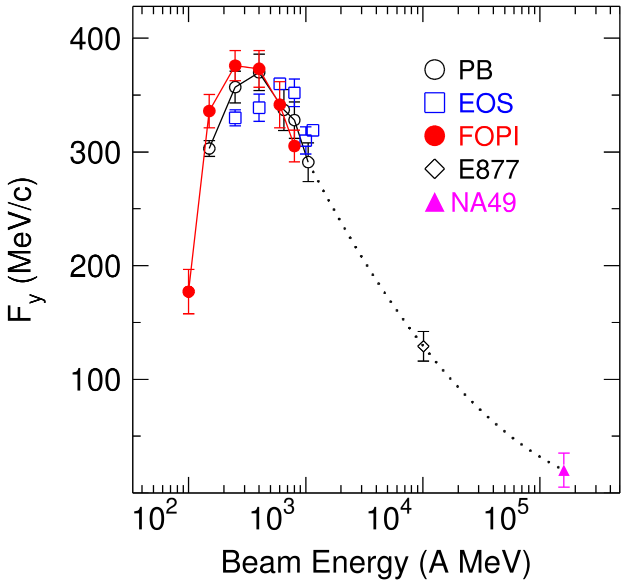

Figure 5.
Energy dependence from SIS to SPS energies of the proton sidewards flow as a function of the beam kinetic energy per nucleon.

final state interaction, and collective flow which is apparent in a distinctly different p_t dependence of v_1 (see [20,19]).

At AGS energy it was shown that in a hadronic cascade code (RQMD) one can indeed reproduce the overall magnitude of the proton directed flow if a repulsive mean field between the nucleons is introduced [17]. The same calculation however fails completely to reproduce the shape of the p_t dependence of the proton directed flow which is on the other hand well matched by a hydrodynamically inspired picture of a sideways moving and expanding fireball [17,20].

The elliptic flow of nucleons, quantified by the coefficient v_2, shows an interesting dependence on beam energy. At lower beam energies it reflects the energy dependence of the nucleon-nucleon interaction which is attractive at very low energies and becomes repulsive in the 50 to 100 MeV/nucleon range. In terms of elliptic flow this is reflected in a change of sign of v_2, i.e. a 90° change in orientation of the ellipse (positive sign: long axis in the reaction plane) and leads to the so-called squeeze-out in the Bevalac/SIS energy regime with dominant nucleon emission perpendicular to the reaction plane. At AGS energy the elliptic flow is small but now oriented along the reaction plane [17] and at SPS energy the elliptic flow is significantly stronger but oriented the same way. Such behavior had been predicted by theory [21] as a consequence of the changing relative importance of shadowing (leading to out-of-plane squeeze-out) and of collective flow related to the pressure build-up early in the reaction. At AGS and higher energies this compression related elliptic flow appears to dominate. The data are by now quantitative enough that a theoretical analysis should be performed to deduce the early pressure build-up.

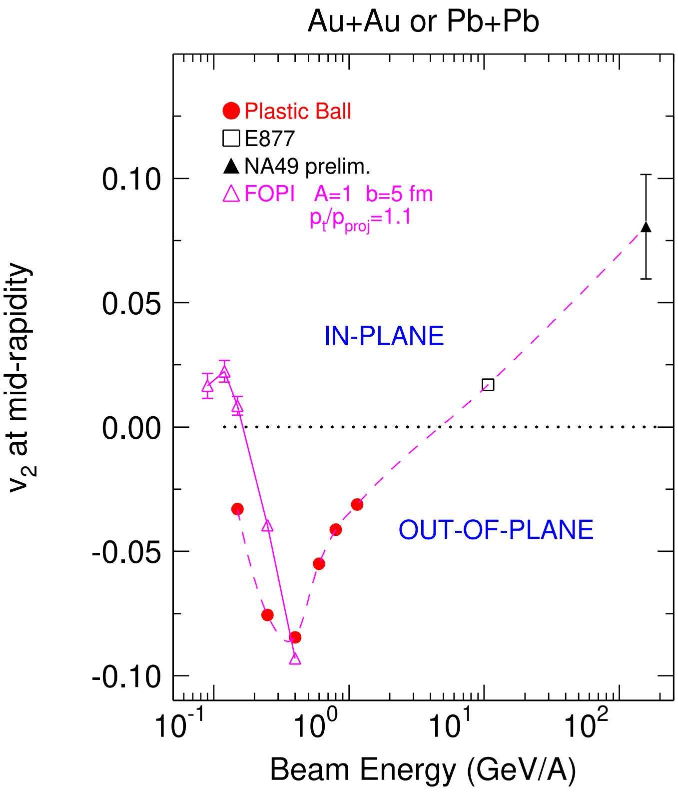

Figure 6.
Energy dependence from SIS to SPS energies of the elliptic flow (second Fourier coefficient).

3.4. Thermal Equilibrium and Freeze-out

At the time of the Quark Matter '96 conference one of us reviewed the evidence for chemical and thermal equilibrium among the hadrons produced in ultra-relativistic collisions between heavy nuclei [22]. The conclusion at that time was that many features of the data indeed imply that a large degree of chemical equilibration is reached both at AGS and SPS energy. Since that time more data have become available (essentially all at SPS energy) and we will provide a brief update on the question of chemical equilibrium. We would like to stress, however, that a final word on this important question can come only after the data have been consolidated and when data cover as much as possible of the full solid angle.

In Table 1 we show an update of presently available particle ratios for Pb+Pb central collisions at SPS energy, along with predictions from a thermal model calculation [23] which is slightly refined compared to our previous model [24]. Fairly good agrement between data and calculations is obtained assuming full chemical (including strangeness) equilibration for temperatures of 160 and 175 MeV, corresponding baryon chemical potentials of 200 and 270 MeV, and no strangeness suppression. In fact, the more consolidated data available now favor the larger baryon chemical potential; we mainly show the calculation with T = 160 MeV and μ_b = 200 MeV as a reference (which best described the preliminary data available at the time of Quark Matter '96). The systematic uncertainties in the particle ratios as witnessed by the differences, e.g., in the $\bar{\Lambda}/\Lambda$ or Ξ^-/Λ ratios from NA49 and WA97 are presently still too large to make a final judgement. We, therefore, feel that the claim of a recent analysis of NA49 data [25] of partial strangeness equilibration is premature.

Table 1
Particle ratios calculated in 2 versions of a thermal model for temperatures of 160 and 175 MeV, and baryon chemical potentials μ_b of 200 and 270 MeV, in comparison to experimental data (with statistical errors in parentheses) for central collisions of Pb+Pb at SPS energy.

Particles	Thermal Model		Experimental Data		
	1	2	exp. ratio	Exp.	y
p-$\bar{\text{p}}$/neg[a]	0.17	0.23	0.23(3)	NA49	0.2-5.6
π^-/π^+	1.04	1.06	1.10(5)	NA49	all
$\bar{\text{p}}$/p[a]	0.086	0.050	0.055(10)	NA44	2.3-2.9
$\bar{\text{p}}$/p[b]	0.099	0.076	0.085(8)	NA49	2.5-3.3
$\bar{\text{d}}$/d	$6.7 \cdot 10^{-3}$	$2.1 \cdot 10^{-3}$	$3.6(8) \cdot 10^{-3}$	NA44	1.9-2.1
K^+/K^-	1.57	1.94	1.61(15)	NA49	2.5-3.3
			1.85(9)	NA44	2.4-3.5
K^0_s/π^-	0.145	0.138	0.125(19)	NA49	all
$\bar{\Lambda}/\Lambda$[a]	0.147	0.115	0.128(12)	WA97	2.3-3.4
$\bar{\Lambda}/\Lambda$[b]	0.17	0.15	0.19(1)	NA49	2.6-3.8
$2\phi/(\pi^+ + \pi^-)$	0.020	0.020	$9.1(10) \cdot 10^{-3}$	NA49	all
Ξ^+/Ξ^-[a]	0.255	0.273	0.266(28)	WA97	2.4-3.4
Ξ^-/Λ[a]	0.114	0.101	0.093(7)	"	"
Ξ^-/Λ[b]	0.093	0.084	0.13(4)	NA49	2.0-2.6
$\Xi^+/\bar{\Lambda}$[a]	0.198	0.239	0.195(23)	WA97	2.4-3.4
Ω^+/Ω^-[a]	0.46	0.68	0.46(15)	"	"
$(\Omega^+ + \Omega^-)/(\Xi^+ + \Xi^-)$[a]	0.154	0.168	0.195(28)	"	"

[a] No feeding from weak decays.
[b] Feeding from weak decays included.

Note that, as discussed above, there is now evidence that, at SPS energy, thermal freeze-out happens at smaller temperature than chemical freeze-out.

In Fig. 7 we show, for SIS, AGS, and SPS energies, the freeze-out parameters deduced from the chemical analysis of particle yields. It is interesting to note that, at the higher energies, the freeze-out points approach the calculated phase boundary [24] while freeze-out parameters for experiments at SIS energies never come close to it.

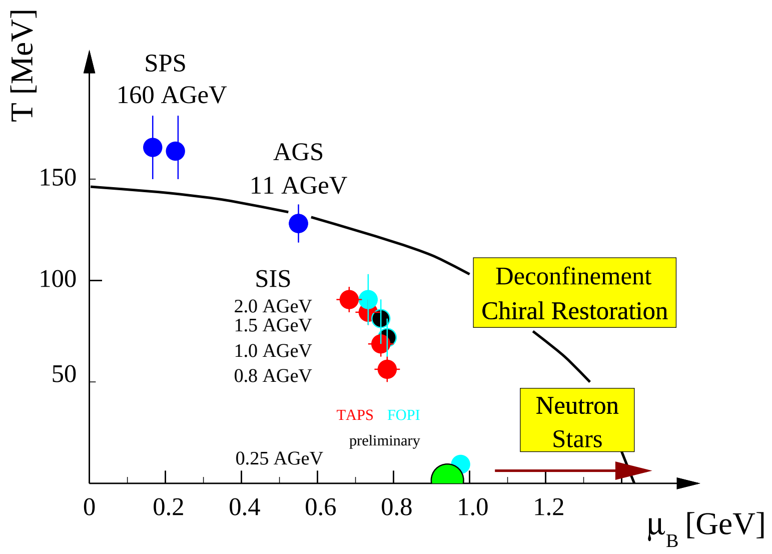

Figure 7.
Freeze-out parameters deduced from the hadro-chemical analysis of particle production yields at SIS, AGS, and SPS energies. At the higher energies the freeze-out points approach the phase boundary.

4. Leptonic Observables

4.1. The dilepton continuum

First results from a measurement of the dilepton continuum at low mass in Pb+Au collisions were shown at the Quark Matter '96 conference [26]. Meanwhile, the CERES collaboration has released the final data [27]. Similar to what was observed for the S+Au data, the electron pair yield in the invariant mass range $0.2 - 2.0$ GeV is enhanced by a factor of $3.5 \pm 0.4(stat.) \pm 0.9(syst.)$ over what is expected from neutral meson decays extrapolating from nucleon-nucleon collisions. The enhancement increases strongly (approximately quadratically) with charged particle multiplicity and, hence, centrality. Most notable is that the observed enhancement seems to be concentrated at low transverse momenta. This is shown in Fig. 8 where, for Pb+Au collisions, inclusive e^+e^- pair transverse momentum spectra are presented for three different pair mass ranges. The spectra are normalized again to charged particle multiplicity. For pair masses less than 0.2 GeV the data agree, as expected, with the sum of the hadron decay contributions. For larger pair masses, especially visible in the mass range between 0.2 and 0.6 GeV, the enhancement is strongest at very low pair transverse momentum.

These results corroborate earlier findings for S+Au collisions of a lepton pair yield which is significantly enhanced compared to expectations for neutral meson decays. The new results, i.e. the strong centrality dependence and the concentration of the enhancement at low pair transverse momenta, should help to distinguish between various models put forward for the interpretation of these data.

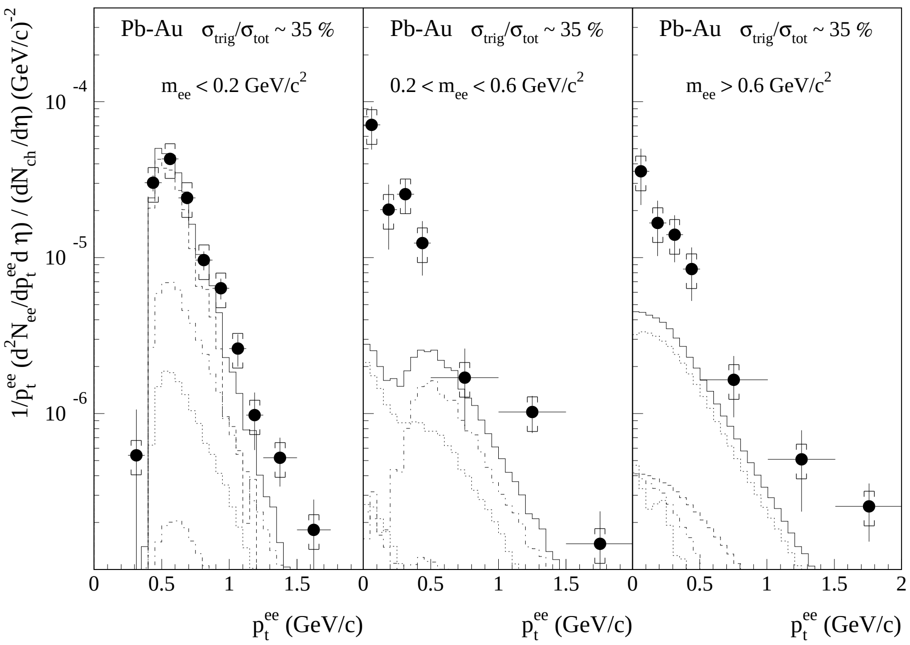

Figure 8.
The dependence on pair transverse momentum of the inclusive lepton-pair continuum for different mass windows. The data are for Pb+Au collisions from the CERES collaboration [27].

4.2. Charmonium suppression

The NA50 collaboration reported anomalous J/Ψ suppression in Pb+Pb collisions at SPS energy at the Quark Matter '96 conference [28]. In 1996 the collaboration increased their data sample on J/Ψ by about a factor of 5, and modified their apparatus to cover a much larger range in centrality. The preliminary results reported at this conference are shown in Fig. 9. Shown here is the ratio of J/Ψ to Drell-Yan production versus the geometrical mean path length L of the J/Ψ or $\bar{c}c$ state traversing the target and projectile matter. The quantity L is, apart from very central collisions where L saturates, a fairly good measure of centrality but, more importantly, can be used to compare various systems ranging from p+A to Pb+Pb collisions.

Prior to data on Pb+Pb collisions the ratio of J/Ψ to Drell-Yan was found to decrease exponentially with L, implying absorption of the J/Ψ or its precursory $/barcc$ state in the nuclear material with an absorption cross section of 6.2 $\pm$0.6 mb. The new data shown in Fig. 9 confirm the findings reported at Quark Matter '96 but now also demonstrate that, for peripheral Pb+Pb collisions i.e. those with L less than about 8 fm, the ratio of J/Ψ to Drell-Yan follows approximately (actually the slope seems somewhat steeper) the same exponential behavior also called 'normal nuclear absorption'. In fact, the data exhibit a rather strong additional suppression setting in at around L = 8 fm. How rapid the onset of anomalous absorption is needs to be studied further. However, it is clear from the correlation between transverse energy and impact parameter or L that fluctuations in transverse energy lead to uncertainties of L (even for very small transverse energy bins) of the order of 1 fm and, hence, no "discontinuity" can be expected in the data over L ranges less than that.

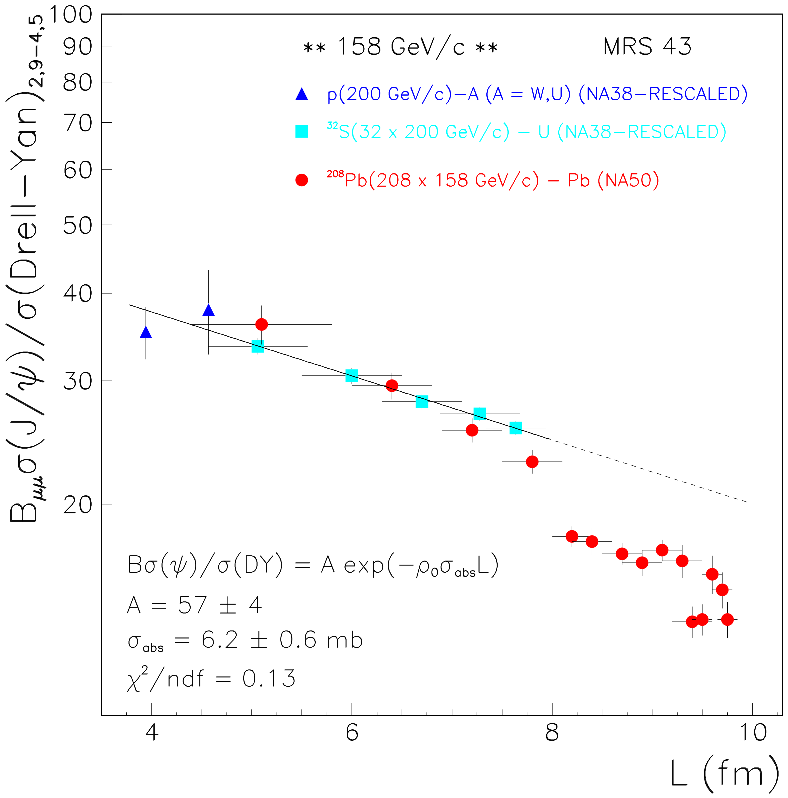

Figure 9.
Anomalous J/Ψ suppression as observed by the NA50 collaboration [29]. For more details see text.

Nevertheless, the most exciting interpretation of the anomalous absorption is that, in the center of the hot and dense fireball formed in the collision, the initially hadronic matter is converted into bubbles of quark-gluon plasma where bound charmonium states cannot survive. Certainly the observations are consistent with this scenario (see, e.g., the talk by Kharzeev [30] at this conference). Alternative explanations have focussed on a scheme in which hadronic comovers break up the J/Ψ (see, e.g., the talk by Vogt [31] at this conference. However, within the framework of such models it turns out rather difficult to explain the complete absorption curve. Furthermore, for the absorption picture to work the comover density must be unrealistically high (on the order of $1/\text{fm}^3$).

5. Summary and Outlook

Over the past year the field has seen significant advances. There is now strong evidence from many experiments that the initially very hot and dense fireball formed in ultra-relativistic nuclear collisions expands with a common flow velocity prior to freeze-out. Other collective features like directed flow and elliptic flow have now been also demonstrated at SPS energy. Both at AGS and SPS energy thermal freeze-out occurs at a temperature close to 120 MeV. Chemical freeze-out seems to occur at AGS energy at nearly the same temperature, while at SPS energy the corresponding temperature is about 170 MeV: apparently chemical freeze-out occurs close to where one expects the phase boundary based on the predictions of lattice QCD and simple bag models. New data from the CERES collaboration have consolidated the picture on an enhanced low mass electron pair continuum, although a real distinction between the various explanations put forward for the nature of the enhancement will probably have to await new data with much improved resolution and statistics. The J/Ψ suppression observed by the Na50 collaboration has not found any convincing explanation in terms of conventional scenarios. Based on this we look into the future with great enthusiasm.

REFERENCES

1. J. Barrette et al., the E877 Collaboration, Phys. Rev. Lett **70**(1993) 299.
2. T. Alber et al., the NA49 Collaboration, Phys. Rev. Lett. **75** (1995) 3814.
3. E. Laermann, Nucl. Phys. **A610** (1996) 1c.
4. J. Barrette et al., the E877 Collaboration, Phys. Rev. **C51**(1995)3309.
5. S. V. Afanasiev et al., NA49 Collaboration, Nucl. Phys. **A610** (1996) 188c.
6. L. Ahle et al., the E802 Collaboration, Nucl. Phys. **A610** (1996) 139c.
7. J. Barrette, the E877 Collaboration, Nucl. Phys. **A610** (1996) 153c.
8. S. Ahmad et al., the E891 Collaboration, Phys. Lett **B382** (1996) 35.
9. M. Aggarwal et al., the WA98 Collaboration, Nucl. Phys. **A610** (1996) 200c.
10. H. Bøggild et al., the NA44 Collaboration, Phys. Lett. **B372** (1996) 339; Phys. Rev. Lett. **78** (1997) 2080.
11. G. Roland, Na49 Collaboration, these proceedings.
12. A. Leonidov, M. Nardi, H. Satz, Nucl. Phys. **A610** (1996) 124c; Z. Physik **C74** (1997) 535.
13. for a discussion, see, *e.g.*, P. Braun-Munzinger, D. Miskowiec, A. Drees, C. Lourenco, Euro. Phys. J. **C1** (1998) 123.
14. F. Ceretto et al., CERES Collaboration, these proceedings.
15. J. Alam, J. Cleymans, K. Redlich, H. Satz, nucl-th/9707042.
16. H. Appelshäuser et al., the NA49 Collaboration, Z. Physik **C** (in press).
17. J. Barrette et al., the E877 Collaboration, Phys. Rev. Lett. **73** (1994) 2532; Phys. Rev. **C55** (1997) 1420; Phys. Rev. **C56** (1997) 3254.
18. T. Wienold for the NA49 Collaboration, Nucl. Phys. **A610** (1996) 76c; H. Appelshäuser et al., preprint nucl.-ex/9711001.
19. S. Voloshin for the E877 Collaboration, these proceedings.
20. J.P. Wessels for the E877 Collaboration, these proceedings.

21. H. Sorge, Phys. Rev. Lett. **78** (1997) 2309.
22. J. Stachel, Nucl. Phys. **A610** (1996) 509c.
23. I. Heppe and J. Stachel, private communication.
24. P. Braun-Munzinger, J. Stachel, J.P. Wessels, N. Xu, Phys. Lett. **B365** (1996) 1.
25. F. Becattini, M. Gazdzicki, J. Sollfrank, hep-ph/9710529.
26. Th. Ullrich et al., the CERES Collaboration, Nucl. Phys. **A610** (1996) 317c.
27. G. Agakichiev et al., the CERES Collaboration, Phys. Lett. **B** in press.
28. M. Gonin et al., NA50 Collaboration, Nucl. Phys. **A610** (1996) 404c.
29. L. Ramello for the NA50 Collaboration, these proceedings.
30. D. Kharzeev, these proceedings.
31. R. Vogt, these proceedings.